

Thermalization and its Breakdown for a Large Nonlinear Spin

Shane P. Kelly*

*Theoretical Division, Los Alamos National Laboratory, Los Alamos, New Mexico 87545, USA and
Department of Physics and Astronomy, University of California Riverside, Riverside, California 92521, USA*

Eddy Timmermans

XCP-5, XCP Division, Los Alamos National Laboratory, Los Alamos, New Mexico 87545, USA

S.-W. Tsai

*Department of Physics and Astronomy, University of California Riverside, Riverside, California 92521, USA
(Dated: October 9, 2019)*

By developing a semi-classical analysis based on the Eigenstate Thermalization Hypothesis, we determine the long time behavior of a large spin evolving with a nonlinear Hamiltonian. Despite integrable classical dynamics, we find the Eigenstate Thermalization Hypothesis is satisfied in the majority of eigenstates and thermalization is generic. The exception is a novel mechanism for the breakdown of thermalization based on an unstable fixed point in the classical dynamics. Using the semi-classical analysis we derive how the equilibrium values of observables encode properties of the initial state. We conclude with a discussion of relevant experiments and the potential generality of this mechanism for the breakdown of thermalization.

In recent years, experiments on ultra cold atoms and trapped ions[1–4] have succeeded in producing quantum systems that, on relevant time scales, are completely isolated from an environment. Surprisingly, many of these experiments find long time behavior that mimic a system coupled to an environment. These experiments prompt the question of thermalization: Given an initial state $|\psi(t=0)\rangle$, a Hamiltonian $H = \sum_n E_n |n\rangle\langle n|$, and an observable O , when and why does the long time average of O :

$$O(t, T) = \frac{1}{T} \int_t^{t+T} d\tau \langle \psi(\tau) | O | \psi(\tau) \rangle \quad (1)$$

lose memory of its initial state? In other words, when does $O(t, T)$, at long time t , depend only on the energy of the initial state?

The eigenstate thermalization hypothesis (ETH)[5–10] attempts to answer this question. Briefly, it states that if A1) $\langle n | O | n \rangle$ changes very little between eigenstates with similar energy; A2) the level spacings, $E_n - E_{n+1}$, are sufficiently small; and A3) the energy uncertainty of the initial state is sufficiently small, then an eigenstate, randomly selected from a micro-canonical ensemble at the energy of the initial state, will describe the long time average observable (LTO): $O(t, T) \approx \langle n | O | n \rangle$ for large t and T .

ETH is often discussed in extended systems where interactions produce chaotic behavior[9], thermalization is described as a process in which a larger subsystem acts as a thermal bath for a smaller one, and the reduced density matrix of the smaller system is approximated as a Gibbs ensemble[7]. In these systems, the standard mechanism for the breakdown of thermalization is the emergence of an extensive set of conserved charges due to underlying integrability[11–13] or a random disorder potential[14–16].

In few mode bosonic systems, micro-canonical thermalization has been investigated using a semi-classical analysis[17–23]. In these works, the loss of initial state memory is explained by the appearance of chaos in the corresponding classical system as opposed to a direct analysis of eigenstates.

In this letter, we explore a similar phenomenon for the long time behavior of a quantum evolution, but for a system which is not extended nor classically chaotic. The model we study is that of an SU(2) spin with large fixed size $|J| > 50$ and evolving with respect to the Hamiltonian $H = -J_x + \frac{\Lambda}{2|J|} J_z^2$, where J_x, J_z and J_y are the canonical SU(2) spin operators, and we assume $\Lambda > 1$. We formulate the question of thermalization for this system by asking: 1) for which initial states do LTOs thermalize and approach a micro-canonical ensemble, and 2) for states that do not thermalize, what is the mechanism that maintains information about the initial state. We focus our analysis on the observables $O = J_x$ and $O = J_z$, and refer to the Supplemental Material for other observables.

This spin Hamiltonian is expected to describe boson tunneling experiments[4, 24], and the theory community has explored its dynamics[25–34]. Particularly relevant results are those relating to a semi-classical analysis[25–28, 31–33, 35], and describe the classical trajectories shown in Fig. 1. These trajectories, and corresponding eigenstates, have two distinct behaviors known as Josephson oscillation and self trapping, and are separated by a separatrix at $E = 1$. Unlike the few-mode boson models, these trajectories are not chaotic and relaxation occurs through quantum effects[31]. Thus, to consider the question of thermalization, we use the correspondence between periodic classical trajectories and eigenstates[36] to access the assumptions required by ETH and answer

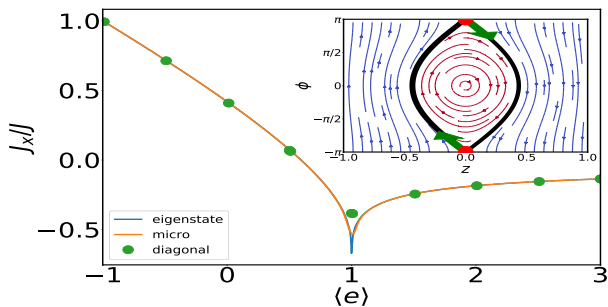


FIG. 1. (Color online) Energy dependence of ensemble expectations values of J_x : The orange line is for the Micro-canonical, while the green dot's are for the diagonal ensembles with initial phase $\phi' = 0$ and increasing $\langle J_z \rangle / J = z'(E)$. The energy dependence of the eigenstate expectation values is also shown. These calculations were performed for $|J| = 1000$ and $\Lambda = 10$. Notice the strong departure of the diagonal ensemble at $E = 1$ from the micro-canonical ensemble. Classical trajectories (inset): the separatrix is shown in black (bold) and separates the circular free-oscillation trajectories (red) from the self-trapping ones (blue). The red dots mark the unstable fixed point at $(z = 0, \phi = \pm\pi)$ and the green arrows mark the unstable directions.

the questions posed above. We find that 1) for initial states with energy sufficiently different from the energy of the separatrix, $E = 1$, the assumptions of ETH are obeyed and observables come to an equilibrium described by a micro-canonical ensemble; and 2) for initial states with energy on the separatrix, the assumptions of ETH do not hold and LTO do not thermalize. We find that the breakdown of thermalization is due to the $E \approx 1$ eigenstates becoming localized in classical phase space. The semi-classical analysis finds that the localization is due to the asymptotically slow classical dynamics near the unstable fixed point shown in Fig. 1. The ubiquity of this semi classical feature suggests that this mechanism for the breakdown of thermalization is a general phenomenon present in other models.

Semi-Classical Picture and ETH: We first consider the case when the assumptions of ETH are valid and the large spin thermalizes. To do so it will be useful to first consider why assumptions of ETH generally imply thermalization. First consider the eigenstate decomposition of the initial state density matrix, $\sum_{nm} c_n c_m |n\rangle \langle m|$. At long times, t and for sufficiently large T , we can expect that only the diagonal terms of the density matrix to contribute to observables[8, 31]:

$$O(t, T) \approx \sum_m |c_m|^2 \langle m| O |m\rangle. \quad (2)$$

If A3) of ETH is true, then $|c_m|^2$ is non zero only in a small energy window. Furthermore, if A1) of ETH holds, then $\langle m| O |m\rangle$ is approximately constant over the eigenstates with significant probability $|c_m|^2$. Finally A2) ensures there are multiple eigenstates in the micro-

canonical ensemble which can be sampled, and we can conclude that a representative eigenstate $\langle n| O |n\rangle$ can be chosen to factor out of the average in Eq. 2 yielding: $O(t, T) \approx \langle n| O |n\rangle$.

We now use a semi-classical analysis to determine when these three assumptions of ETH hold for the nonlinear spin Hamiltonian. The semi-classical analysis is based on a Wigner-function formalism in which states and operators are represented as functions, $W(z, \phi)$ and $O(z, \phi)$, of z , the eigenvalue of $J_z/|J|$, and its conjugate momentum ϕ . In this formalism, the observables J_z and J_x are given by $|J|z$ and $|J|\sqrt{1-z^2} \cos(\phi)$ respectively, and the Hamiltonian is written as:

$$\frac{H(z, \phi)}{|J|} = \frac{\Lambda}{2} z^2 - \sqrt{1-z^2} \cos(\phi) \quad (3)$$

The expectation values of a state $W(z, \phi)$ with an observable $O(z, \phi)$ is computed with:

$$\langle \psi | O | \psi \rangle = \frac{1}{4\pi} \int_{-1}^1 \int_{-\pi}^{\pi} dz d\phi W(z, \phi) O(z, \phi). \quad (4)$$

We use the set of spin coherent states as our initial states because they are regularly created in experiments[4, 24]. In the Wigner-function formalism these states are represented by Gaussian distributions (see [37] for specific form) that become more localized around a mean z' and a mean ϕ' as the size of the spin, $|J|$, is increased. Since a state which is more local around a specific z' and ϕ' has smaller energy uncertainty, assumption A3) of ETH is satisfied when $|J|$ is sufficiently large.

We now consider when assumptions A1) and A2) hold by constructing the Wigner functions of the eigenstates via a semi-classical analysis. The zeroth order classical analysis treats Eq. 3 as a classical Hamiltonian which yields the periodic trajectories depicted in Fig. 1. Fig. 1 shows two distinct types of periodic trajectories depending on the energy: for $E < 1$, the trajectories known as Josephson oscillation[25] occur in which z and ϕ periodically oscillates around a stable fixed point at $(z, \phi) = (0, 0)$, while for $E > 1$ trajectories called self trapping[38] occur in which z does not change sign, and ϕ monotonically increases ($z < 0$) or decreases ($z > 0$) depending on the sign of z . At $E = 1$, there is a separatrix separating the two dynamical behaviors.

Using the correspondence between classical periodic trajectories and eigenstates[36], the eigenstate Wigner-functions (EWF) with energy E can be written as $\rho_E(z, \phi) = w(E) \delta(H(z, \phi) - E)$, where $w(E)$ is the normalization of the eigenstate with energy E . The quantized energy levels, $E = E_n$, are then determined by the rule[28] stating that the area swept out by the eigenstate trajectories is quantized to $2\pi/|J|$. Thus, the energy difference between the eigenstate trajectories goes to 0 as $|J|$ is increased, and assumption A2) of ETH holds true.

Considering assumption A1), we first identify that the Hamiltonian in Eq. 3 has two distinct types of eigenstates corresponding to the Josephson oscillation and the self trapping trajectories. The self trapping eigenstates are further structured because, for a given energy $E > 1$, there are two disconnected trajectories depending on the initial sign of z . These two trajectories will be identified with the sign of z and their associated EWFs are calculated by selecting the correct trajectory when inverting $H(z, \phi)$:

$$\rho_{E\pm}(z, \phi) = w(E) \left| \frac{dH(z, \phi)}{dz} \right|^{-1} \delta(z \pm |H^{-1}(E, \phi)|) \quad (5)$$

At lowest order in a semi-classical expansion, these two trajectories correspond to two degenerate eigenstates, while at higher order the degeneracy is lifted[39] with splitting exponentially decreasing with $|J|$. Since this splitting is exponentially small, we will ignore it and assume all measurements occur before its dynamics are realized ($t < T_t \approx e^{|J|}$).

With EWFs identified, we are now able to assess the validity of assumption A1) of ETH. For the Josephson oscillation eigenstates, the difference between two neighboring eigenstate trajectories decreases to 0 as $|J|$ is increased. Thus, we expect the eigenstate observables will be smooth in energy for $-1 < E < 1$. The same is also true in each of the $\text{sgn}(z) = \pm 1$ branches of the self trapping eigenstates with $E > 1$. On the separatrix, the self trapping trajectories meet the free oscillating ones, a discontinuity emerges, and non analytic behavior of the eigenstate observables is expected. The smooth behavior away from $E = 1$ along with the non-analytic behavior at $E = 1$ has been identified previously[25, 40] and we confirm for J_x in Fig. 1 .

Thus, we find that away from $E = 1$ and for large enough $|J|$, the assumptions of ETH hold, and we expect the LTOs to be described by a micro-canonical ensemble. While for eigenstates with energy $E \approx 1$, assumption A1) of ETH does not hold, and additional consideration is required to understand the long time behavior.

Numerical Analysis of the Diagonal Ensemble: From the analysis of the previous section we expect initial coherent states with z' and ϕ' away from the separatrix to show thermal behavior at long times. That is, we expect the LTO to 1) depend solely on conserved quantities (the energy and initial sign of z for $E > 1$), 2) match a micro-canonical ensemble and 3), for large enough spin, to match a characteristic eigenstate selected from the micro-canonical ensemble. To confirm these expectations, we focus on initial coherent states and compute LTOs using exact diagonalization and Eq. 2. In the left column of Fig. 2, we show the long time expectation of J_x and J_z for a set of initial coherent states with different ϕ' , but with energy fixed to $E = 0.5$ in the Josephson Oscillation regime. It demonstrates that the LTO cannot

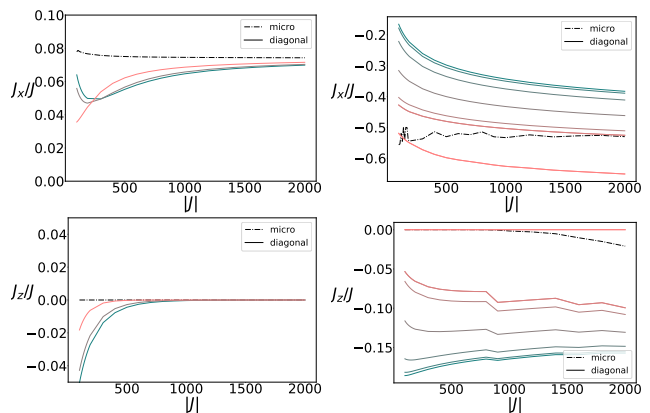


FIG. 2. (Color online) Micro-canonical and Diagonal Ensemble Expectation Values as a function of $|J|$ and ϕ' for $E = 0.5$ (1st column) and $E = 1$ (second column). The color indicates the initial phase ϕ' where in the second column it ranges from 0 (dark blue) to π (bright pink). For $E = 0.5$, as $|J|$ increases the energy level spacing increases, assumptions A2) and A3) of ETH becomes more valid and the dependence of diagonal ensemble expectation value on the initial phase is lost. While for $E = 1$, memory of the initial state is maintained. These calculations were done with $\Lambda = 10$

distinguish between initial states with different ϕ' , and thus memory of the initial state is lost.

We next identify if a micro-canonical ensemble, and a characteristic eigenstate describe the LTOs. The micro-canonical ensemble is constructed as a Gaussian distribution in the energy eigenstates with a projection onto one of the self trapping branches (see SM Sec.2 for numerical details). We take the eigenstate with maximum amplitude as the characteristic eigenstate to be compared with the LTO. Fig. 1 depicts how the expectation value of J_x for the micro-canonical ensemble, the characteristic eigenstate, and the diagonal ensemble depend on energy, and confirms that the micro-canonical ensemble and the characteristic eigenstate describe the LTO computed by the diagonal ensemble for $E \neq 1$.

Close the $E = 1$, the micro-canonical ensemble and the characteristic eigenstate no longer match LTOs. Failure of the initial states at $E = 1$ to thermalize is further demonstrated in the right column of Fig. 2, which shows a dramatic dependence of the diagonal ensemble expectation value on the initial phase, ϕ' . This does not invalidate ETH because assumption A1) of ETH does not hold for these eigenstates.

Semi-Classical Analysis of the Breakdown of Thermalization: To better understand this breakdown of thermalization we investigate, using the semi-classical analysis, how the $E \approx 1$ eigenstates affect the LTO of the initial coherent states with $E \approx 1$. We begin by calculating the diagonal ensemble and its expectation values for the initial coherent states used above. Semi-classically[28] this

diagonal ensemble is given as:

$$\rho_{diag} = \frac{1}{4\pi} \int_{-\pi}^{\pi} \int_{-\pi}^{\pi} dz d\phi W_c(z, \phi, z', \phi') \rho_{E,s}(z, \phi) \quad (6)$$

where W_c is the initial coherent state Gaussian distribution centered around z' and ϕ' with variance $\sim \frac{1}{J}$, and the EWF, $\rho_{E,\pm}$, is given by Eq. 5. This integral can be computed when $(z', \phi') \neq (0, \pi)$ since the Jacobian $\left| \frac{dH(z, \phi)}{dz} \right|^{-1}$ is approximately constant in the vicinity of z' and ϕ' . Performing the Dirac delta and Gaussian integrations yields:

$$\rho_{diag}(\phi', z', E, s) \sim e^{-\frac{E-H(\phi', z')}{2\sigma^2(\phi', z')} + \text{Ln}(w(E))} \quad (7)$$

where $w(E)$ is the eigenstate normalization, and the energy variance $\sigma(\phi', z')$ scales with $|J|$ as $\sim \frac{1}{\sqrt{|J|}}$ with proportionality dependent[41] on ϕ' and z' .

To calculate the LTOs, one must convolve the diagonal ensemble with the eigenstate expectation values:

$$O_{diag}(\phi', z') = \int_{-1}^{\Lambda/2} dE \sum_s \rho_{diag}(\phi', z', E, s) O(E, s) \quad (8)$$

where the sum over s is the sum over self trapping states when $E > 1$ and a fixed $s = 0$ for $E < 1$, and $O(E, s)$ is the eigenstate expectation value calculated using Eq. 4 with $W(z, \phi) = \rho_{E,s}(z, \phi)$.

Understanding this integral, and consequently why the LTOs encode information about the initial phase ϕ' , requires understanding the structure of the eigenstates and their EWFs. While an EWF is constrained to an equal energy surface, the shape of the energy surface affects how the EWF is distributed within the energy surface. This is captured by the Jacobian, $\left| \frac{dH(z, \phi)}{dz} \right|$, which appears in Eq. 5 due to the transformation of the energy delta function to phase space coordinates. Take the $s = 1$ self trapping eigenstate for example. If one integrates out z using the delta function, the Jacobian $\left| \frac{dH}{dz} \right|(E, \phi) = \left| \frac{d\phi}{dt} \right|(E, \phi)$ weighs the EWF. Therefore, the EWF will have more weight in regions where ϕ is changing slower in time.

On the separatrix, $E = 1$, the classical spin comes to a complete stop on the unstable fixed point; the Jacobian limits to 0, $\lim_{E \rightarrow 1} \lim_{\phi \rightarrow \pi} \left| \frac{dH}{dz} \right|(E, \phi) = 0$; and the EWFs with $E \rightarrow 1$ become localized on the unstable fixed point: $\rho_{E \rightarrow 1}(z, \phi) \approx \delta(z) \delta(\phi - \pi)$. The singularity of this localization result in the non-analytic behavior of the eigenstate expectation values near $E = 1$ (see for example J_x in Fig. 1).

This singular localization also produces a non-analyticity in the eigenstate overlaps for the set of initial coherent states with $E \approx 1$, but $\phi' \neq \pi$. Since these initial states have Wigner functions localized around ϕ' and $z' = H^{-1}(E = 1, \phi')$ and the EWFs for $E \approx 1$ are localized around $\phi = \pi \neq \phi'$ and $z = 0 \neq z'$, their overlap integrals in Eq. 8 will vanish.

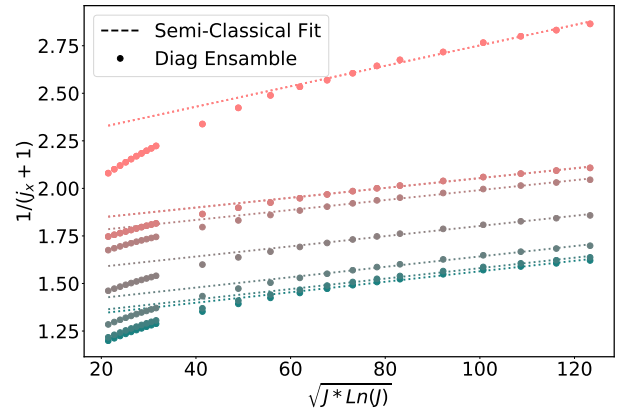


FIG. 3. (Color online) Classical fit to exact numerical calculations of diagonal ensemble. This plot shows the $\sqrt{|J| \text{Ln}|J|}$ scaling of $j_x = J_x/J$ for the diagonal ensemble of a set of initial states with energy $E = 1$ and different ϕ' and $|J|$. The dots are computed using exact diagonalization and the color indicates the initial ϕ' as in Fig. 2. Eq. 9 predicts $\sqrt{|J| \text{Ln}|J|}$ and the linear dashed lines are given by Eq. 9 with $F(\phi')$ fit to match the exact calculations for $|J| > 500$.

These two non-analyticities are integrated over in Eq. 8 and result in the memory effects depicted in Fig. 2. In one limit, an initial coherent state with $\phi' \approx \pi$ will overlap the unstable fixed point eigenstate at $E = 1$, and the LTOs will closely match the observables of that same eigenstate ($J_z = 0$ and $J_x = -1$). In the other limit, when the initial ϕ' is away from π , the initial coherent state will have negligible overlap with the $E = 1$ eigenstate, the LTOs will depart from the observables of the $E = 1$ eigenstate. This is depicted in Fig. 2, in which the closer ϕ' is to π , the closer $j_z = J_z/J$ and $j_x = J_x/J$ approach 0 and -1 respectively.

To capture this behavior analytically, we perform a saddle point expansion for the integral Eq. 8, and evaluate the integrand at the peaks of ρ_{diag} , given in Eq. 7. To calculate the integrands that give the eigenstate normalization, $w(E)$, and the eigenstate observables, $O(E, s)$, we perform an expansion of the trajectories around the unstable fixed point to second order in (z, ϕ) . The phase, ϕ' , and size, $|J|$, dependence of diagonal ensemble observables are then derived as[42]:

$$j_{z,diag}(|J|, E = 1, \phi') = \frac{4\pi\sqrt{(\Lambda-1)}}{3\Lambda \text{Ln}[F(\phi')|J| \text{Ln}[|J|]]} \quad (9)$$

$$j_{x,diag}(|J|, E = 1, \phi') = -1 + \frac{1}{\sqrt{F(\phi')|J| \text{Ln}[|J|] }} \frac{3 + \Lambda}{3(\Lambda - 1)}$$

where the factor $F(\phi') = [2\sigma(z', \phi')^2 |J|]^{-1}$, $j_{x(z)} = J_{x(z)}/J$, and z' is fixed by energy $z' = H^{-1}(E = 1, \phi')$. The factor $F(\phi')$ is constant in $|J|$ but has a non trivial dependence on the initial phase ϕ' via $\sigma(z', \phi')$, the energy variance of the coherent state. This non trivial dependence in ϕ' describe the memory effects shown in

Fig. 2 for the initial states with $\phi' \neq \pi$. For the initial states with $\phi' \approx \pi$ the approximation for ρ_{diag} given in Eq. 7 breaks down, and the results in Eq. 9 become invalid. For these states, a different approximation is required and results in LTO closer to the unstable fix point[28, 33]. While the exact diagonal ensemble for J_z becomes numerically unstable for large $|J|$, we can still compare exact results for J_x with Eq. 9. This comparison is shown in Fig. 3, where the $\sqrt{|J|} \text{Ln}[|J|]$ scaling is confirmed. Note that the breakdown of thermalization is a quantum effect which is lost in the $J \rightarrow \infty$ classical limit.

Discussion and Possible Experimental Realizations:

Above we discussed how, for the large non-linear spin with energy $E \neq 1$, the assumptions of ETH hold and the spin thermalizes, while for $E = 1$ the spin does not thermalize. We found that spin fails to thermalize for $E \approx 1$ because the slow dynamics of an unstable fixed point produces eigenstates localized in the classical phase space. These results are valid when J is finite and quantum effects are present, but large enough ($J > 200$) that assumption A2) and A3) hold.

The appearance of unstable fixed points in semi-classical dynamics is ubiquitous, and we expect this mechanism for the breakdown of thermalization to be general. Quantum systems with integrable classical dynamics offer the simplest generalization, because the correspondence between classical trajectories and eigenstates still holds and the analysis above can be easily repeated. For classically chaotic systems, the same correspondence does not hold, but the eigenstates must still capture the slow dynamics in the semi-classical limit. Thus, it is reasonable to still expect the existence of a set of eigenstates that are localized on the unstable classical fixed points and responsible for the slow dynamics.

This mechanism for the breakdown of thermalization may be observable in ultra cold BECs[4, 43] in which the bosons can be condensed into one of two modes such as two different hyperfine states. A spin boson mapping then yields the non-linear spin Hamiltonian, where the parameter Λ is a ratio between the bosonic interaction energy and the energy associated with the tunneling between the two modes. This mapping hides additional modes that can act as a bath and hide the non thermal behavior discussed above. Thus, for an experiment to observe this behavior, the time scale associated with the coupling to these modes must be longer than the relaxation time of these spins. Given such a limit, the non thermal behavior could then be observed by preparing different initial states with $E \approx 1$ and different ϕ' and observing the LTOs of J_z or J_x . Previous work has suggested this limit may exist[31, 32], while other work[44] found the addition of other modes will produce a different form of non ergodic behavior. It will be interesting to investigate if the two forms of non ergodic dynamics are related.

Acknowledgments: This work was supported in part by the NSF under Grant No. DMR-1411345, S. P. K. acknowledges financial support from the UC Office of the President through the UC Laboratory Fees Research Program, Award Number LGF-17- 476883. The research of E. T. in the work presented in this manuscript was supported by the Laboratory Directed Research and Development program of Los Alamos National Laboratory under project number 20180045DR.

* skell013@ucr.edu

- [1] Immanuel Bloch, Jean Dalibard, and Wilhelm Zwerger, “Many-body physics with ultracold gases,” *Rev. Mod. Phys.* **80**, 885–964 (2008).
- [2] Andrew D. Ludlow, Martin M. Boyd, Jun Ye, E. Peik, and P. O. Schmidt, “Optical atomic clocks,” *Rev. Mod. Phys.* **87**, 637–701 (2015).
- [3] J. P. Shaffer, S. T. Rittenhouse, and H. R. Sadeghpour, “Ultracold Rydberg molecules,” *Nature Communications* **9**, 1965 (2018).
- [4] Tilman Zibold, Eike Nicklas, Christian Gross, and Markus K. Oberthaler, “Classical Bifurcation at the Transition from Rabi to Josephson Dynamics,” *Physical Review Letters* **105**, 204101 (2010).
- [5] J. M. Deutsch, “Quantum statistical mechanics in a closed system,” *Phys. Rev. A* **43**, 2046–2049 (1991).
- [6] Mark Srednicki, “Chaos and quantum thermalization,” *Phys. Rev. E* **50**, 888–901 (1994).
- [7] Marcos Rigol, Vanja Dunjko, and Maxim Olshanii, “Thermalization and its mechanism for generic isolated quantum systems,” *Nature* **452**, 854–858 (2008).
- [8] Luca D’Alessio, Yariv Kafri, Anatoli Polkovnikov, and Marcos Rigol, “From quantum chaos and eigenstate thermalization to statistical mechanics and thermodynamics,” *Advances in Physics* **65**, 239–362 (2016).
- [9] Joshua M. Deutsch, “Eigenstate Thermalization Hypothesis,” *Rep. Prog. Phys.* **81**, 082001 (2018), [arXiv:1805.01616](https://arxiv.org/abs/1805.01616).
- [10] R. V. Jensen and R. Shankar, “Statistical Behavior in Deterministic Quantum Systems with Few Degrees of Freedom,” *Phys. Rev. Lett.* **54**, 1879–1882 (1985).
- [11] Anatoli Polkovnikov, Krishnendu Sengupta, Alessandro Silva, and Mukund Vengalattore, “Colloquium: Nonequilibrium dynamics of closed interacting quantum systems,” *Rev. Mod. Phys.* **83**, 863–883 (2011).
- [12] Murray T. Batchelor and Angela Foerster, “Yang–Baxter integrable models in experiments: From condensed matter to ultracold atoms,” *J. Phys. A: Math. Theor.* **49**, 173001 (2016).
- [13] Amy C. Cassidy, Charles W. Clark, and Marcos Rigol, “Generalized Thermalization in an Integrable Lattice System,” *Phys. Rev. Lett.* **106**, 140405 (2011).
- [14] John Z. Imbrie, Valentina Ros, and Antonello Scardicchio, “Local integrals of motion in many-body localized systems,” *Annalen der Physik* **529**, 1600278 (2017).
- [15] Rahul Nandkishore and David A. Huse, “Many-Body Localization and Thermalization in Quantum Statistical Mechanics,” *Annual Review of Condensed Matter Physics* **6**, 15–38 (2015).

- [16] Dmitry A. Abanin, Ehud Altman, Immanuel Bloch, and Maksym Serbyn, “Colloquium: Many-body localization, thermalization, and entanglement,” *Rev. Mod. Phys.* **91**, 021001 (2019).
- [17] Igor Tikhonenkov, Amichay Vardi, James R. Anglin, and Doron Cohen, “Minimal Fokker-Planck Theory for the Thermalization of Mesoscopic Subsystems,” *Phys. Rev. Lett.* **110**, 050401 (2013).
- [18] Geva Arwas, Amichay Vardi, and Doron Cohen, “Superfluidity and Chaos in low dimensional circuits,” *Scientific Reports* **5**, 13433 (2015).
- [19] Christine Khripkov, Doron Cohen, and Amichay Vardi, “Thermalization of Bipartite Bose–Hubbard Models,” *J. Phys. Chem. A* **120**, 3136–3141 (2016).
- [20] Christine Khripkov, Amichay Vardi, and Doron Cohen, “Semiclassical theory of strong localization for quantum thermalization,” *Phys. Rev. E* **97**, 022127 (2018).
- [21] Geva Arwas and Doron Cohen, “Chaos and two-level dynamics of the atomtronic quantum interference device,” *New J. Phys.* **18**, 015007 (2016).
- [22] Geva Arwas and Doron Cohen, “Chaos, metastability and ergodicity in Bose-Hubbard superfluid circuits,” *AIP Conference Proceedings* **1912**, 020001 (2017).
- [23] Geva Arwas and Doron Cohen, “Monodromy and chaos for condensed bosons in optical lattices,” *Phys. Rev. A* **99**, 023625 (2019).
- [24] Helmut Strobel, Wolfgang Muessel, Daniel Linnemann, Tilman Zibold, David B. Hume, Luca Pezze, Augusto Smerzi, and Markus K. Oberthaler, “Fisher information and entanglement of non-Gaussian spin states,” *Science* **345**, 424–427 (2014).
- [25] S. Raghavan, A. Smerzi, S. Fantoni, and S. R. Shenoy, “Coherent oscillations between two weakly coupled Bose-Einstein condensates: Josephson effects, pi oscillations, and macroscopic quantum self-trapping,” *Physical Review A* **59**, 620–633 (1999).
- [26] A. Micheli, D. Jaksch, J. I. Cirac, and P. Zoller, “Many-particle entanglement in two-component Bose-Einstein condensates,” *Physical Review A* **67**, 013607 (2003).
- [27] Khan W. Mahmud, Heidi Perry, and William P. Reinhardt, “Quantum phase-space picture of Bose-Einstein condensates in a double well,” *Physical Review A* **71**, 023615 (2005).
- [28] Maya Chuchem, Katrina Smith-Mannschott, Moritz Hiller, Tsampikos Kottos, Amichay Vardi, and Doron Cohen, “Quantum dynamics in the bosonic Josephson junction,” *Physical Review A* **82**, 053617 (2010).
- [29] Yixiao Huang, Wei Zhong, Zhe Sun, and Xiaoguang Wang, “Fisher-information manifestation of dynamical stability and transition to self-trapping for Bose-Einstein condensates,” *Physical Review A - Atomic, Molecular, and Optical Physics* **86**, 1–7 (2012).
- [30] M. Lapert, G. Ferrini, and D. Sugny, “Optimal control of quantum superpositions in a bosonic Josephson junction,” *Physical Review A - Atomic, Molecular, and Optical Physics* **85**, 1–13 (2012).
- [31] Christine Khripkov, Doron Cohen, and Amichay Vardi, “Temporal fluctuations in the bosonic Josephson junction as a probe for phase space tomography,” *J. Phys. A: Math. Theor.* **46**, 165304 (2013).
- [32] Izabella Lovas, József Fortágh, Eugene Demler, and Gergely Zaránd, “Entanglement and entropy production in coupled single-mode Bose-Einstein condensates,” *Phys. Rev. A* **96**, 023615 (2017).
- [33] R. Mathew and E. Tiesinga, “Phase-space mixing in dynamically unstable, integrable few-mode quantum systems,” *Phys. Rev. A* **96**, 013604 (2017).
- [34] Shane P. Kelly, Eddy Timmermans, and S.-W. Tsai, “Detecting macroscopic indefiniteness of cat states in bosonic interferometers,” *Phys. Rev. A* **100**, 032117 (2019).
- [35] Anatoli Polkovnikov, “Phase space representation of quantum dynamics,” , 1–92 (2009).
- [36] Martin C. Gutzwiller, “Periodic Orbits and Classical Quantization Conditions,” *Journal of Mathematical Physics* **12**, 343–358 (1971).
- [37] See Supplemental Material sec V at
- [38] Michael Albiez, Rudolf Gati, Jonas Fölling, Stefan Hunsmann, Matteo Cristiani, and Markus K. Oberthaler, “Direct observation of tunneling and nonlinear self-trapping in a single bosonic Josephson junction,” *Physical Review Letters* **95**, 010402–010402 (2005).
- [39] Tadeusz Pudlik, Holger Hennig, Dirk Witthaut, and David K. Campbell, “Tunneling in the self-trapped regime of a two-well BEC,” arXiv:1409.0769 [cond-mat, physics:quant-ph] (2014), arXiv:1409.0769 [cond-mat, physics:quant-ph].
- [40] S. F. Caballero Benitez, V. Romero-Rochin, and R. Paredes, “Delocalization to self-trapping transition of a Bose fluid confined in a double well potential. An analysis via one- and two-body correlation properties,” *Journal of Physics B: Atomic, Molecular and Optical Physics* **43**, 115301–115301 (2009).
- [41] See SM, Sec V at . . . for exact dependence.
- [42] See SM Sec III for $W(E)$, Sec V for $O(E, s)$, Sec IV for the saddle point expansion and Sec VI for final derivation of $J_{x(z), (diag)}(\phi', E = 1)$.
- [43] W. Muessel, H. Strobel, D. Linnemann, T. Zibold, B. Juliá-Díaz, and M. K. Oberthaler, “Twist-and-turn spin squeezing in Bose-Einstein condensates,” *Phys. Rev. A* **92**, 023603 (2015).
- [44] Alessio Lerose, Jamir Marino, Bojan Žunkovič, Andrea Gambassi, and Alessandro Silva, “Chaotic Dynamical Ferromagnetic Phase Induced by Nonequilibrium Quantum Fluctuations,” *Phys. Rev. Lett.* **120**, 130603 (2018).

Supplemental Materials

I) Large-J Scaling At Different Energies and for Different Observables

Thermalization in the Self-Trapping Limit

In Fig. S1, we demonstrate the validity of the ETH for $E=3$.

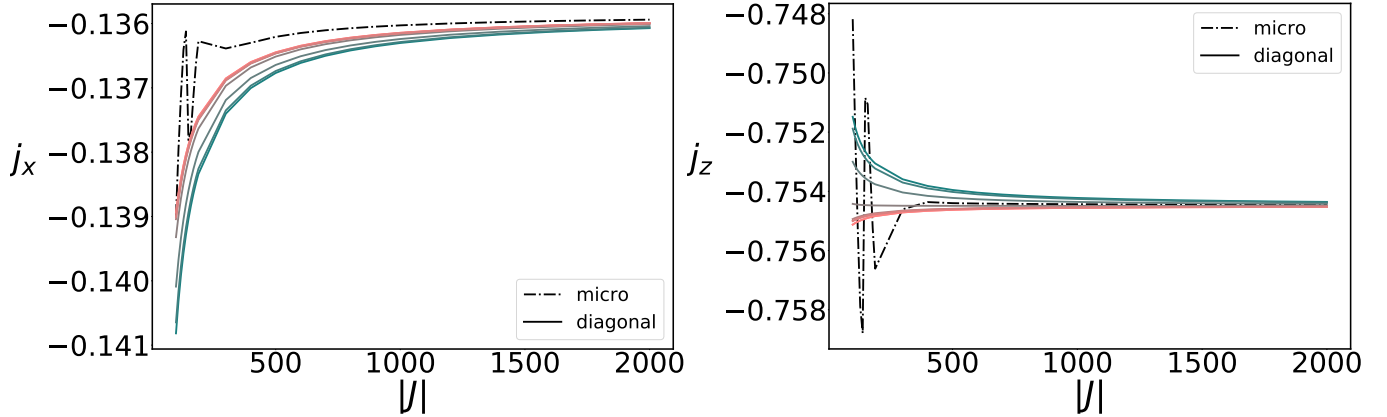


FIG. S1. (Color online) These plots demonstrate the validity of ETH in the self trapping limit for a fixed energy of $E = 3$. The different colors corresponds to different values of ϕ' : blue (darker) $\phi = 0$, pink (lighter) $\phi = \pi$. The dashed line is for the micro-canonical ensemble.

Ensemble Averages v.s. Energy

In this section we repeat a similar analysis done in Fig.1 in the main text for the observables J_z , J_x^2 , J_y^2 and J_z^2 . The results are shown in Figure S2. Each observable shows a non analyticity in the eigenstate observable as a function of energy. J_z shows a discontinuity while, the square observables show a cusp approaching the fixed point value.

II) Numerical Details of Exact Construction of Micro-Canonical Ensembles

In the main text we discuss the use of exact diagonalization to construct the diagonal ensemble and micro-canonical ensemble. We use standard algorithms BLAS and LAPACK algorithms. The one subtlety is the identification of the two degenerate self trapping trajectories. We find that these algorithms naturally find a basis in which there is no tunneling between the two self trapping eigenstates. We then identify $s = \pm 1$ by the sign of $\langle J_z \rangle$ of the produced eigenstate. To confirm a lack of tunneling in the produced degenerate basis, we compute the overlap $\sum_{s, j_z > 0} |\langle s | j_z \rangle|^2$. If the overlap is close to 1 then we know there is very little tunneling between the two self trapping trajectories. Note for the diagonal ensemble $\sum_n \rho_n |n\rangle \langle n|$, we use the non-tunneling degenerate basis, and thus treat the sign of J_z as a quasi conserved integral of motion.

III) Semi-Classical Eigenstates and Eigenstate normalization

. In the main text we defined the semi-classical eigenstate Wigner function (EWF) as:

$$\rho_E(z, \phi) = \omega(E) \delta(H(z, \phi) - E) \quad (S1)$$

where the Hamiltonian is given as:

$$H = \frac{\Lambda z^2}{2} - \sqrt{1 - z^2} \cos(\phi), \quad (S2)$$

and the normalization $\omega(E)$ is given as:

$$\omega(E)^{-1} = \int \int dz d\phi \delta(E - H(z, \phi)). \quad (S3)$$

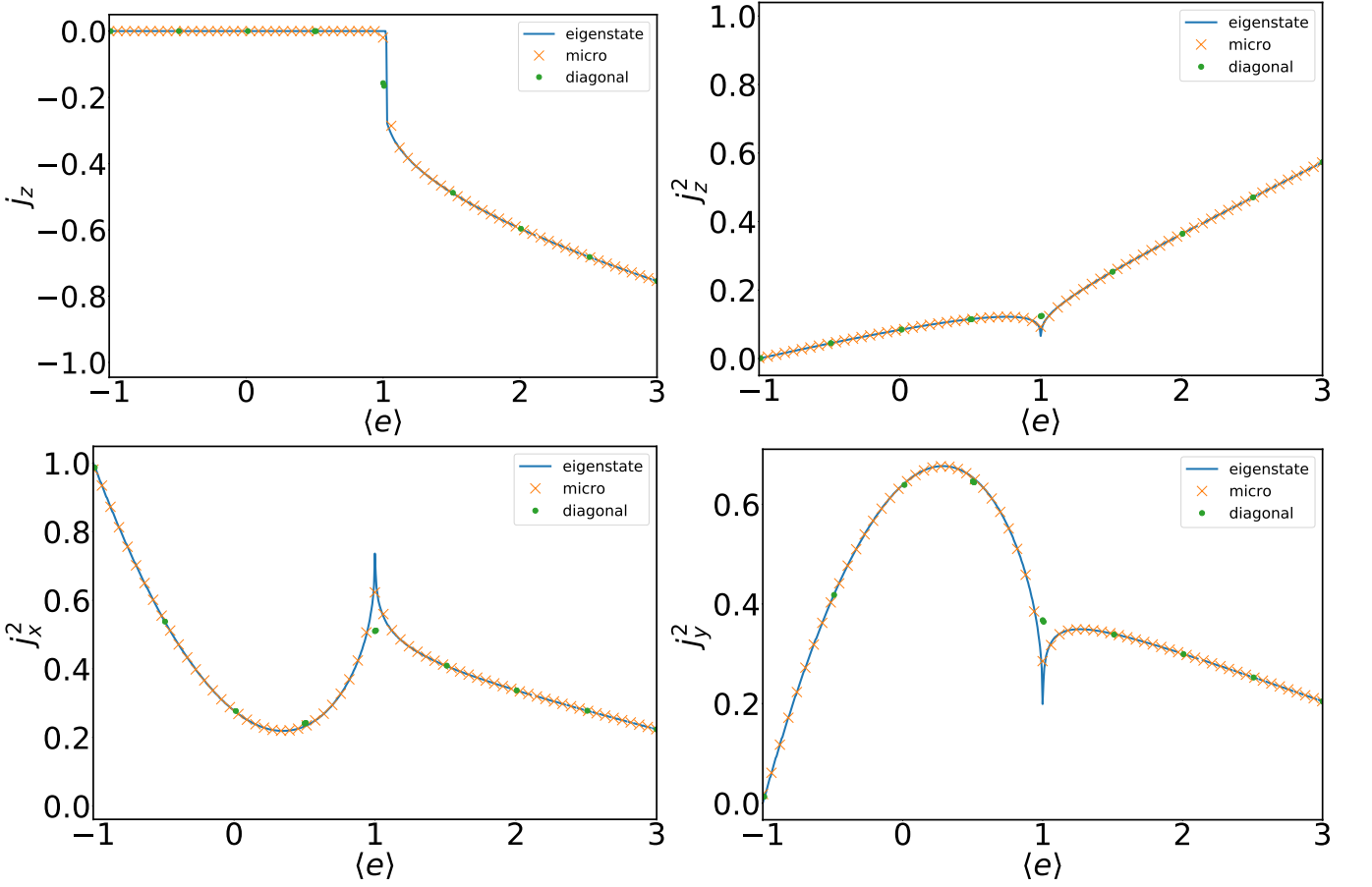


FIG. S2. These plots demonstrate the validity of ETH in the self trapping and free oscillating limit, but it fails on the separatrix ($E=1$).

To compute this integral, we focus on the energy close to the separatrix, $E = 1 \pm |\delta|$, and expand the Hamiltonian around $E = 1$:

$$H - 1 = \frac{\Lambda - 1}{2} z^2 - \frac{(\phi - \pi)^2}{2} \quad (\text{S4})$$

Close to the unstable fixed point the trajectories trace out a hyperbola:

$$z = \pm \sqrt{\frac{2}{\Lambda - 1}} \sqrt{\frac{\phi^2}{2} + (E - 1)} \quad (\text{S5})$$

$$\phi = \sqrt{2(1 - E) + (\Lambda - 1)z^2}$$

The Jacobian for both these trajectories are:

$$\left| \frac{dH}{dz} \right| = (\Lambda - 1)z = \sqrt{(\Lambda - 1)} \sqrt{2(E - 1) + \phi^2} \quad (\text{S6})$$

$$\left| \frac{dH}{d\phi} \right| = \phi = \sqrt{(\Lambda - 1)} \sqrt{\frac{2(1 - E)}{(\Lambda - 1)} + z^2}.$$

Since the the inverse Jacobians, $\left| \frac{dH}{d\phi} \right|^{-1}$ and $\left| \frac{dH}{dz} \right|^{-1}$, contribute the most near the unstable fixed point and we can expand the integrand for $\omega(E)^{-1}$ near them and write:

$$\omega(1 + |\delta|)^{-1} = \int_{-r_+}^{r_+} \left| \frac{dH}{dz} \right|^{-1} (\phi, \delta) + C_+ \quad (\text{S7})$$

$$\omega(1 - |\delta|)^{-1} = \int_{-r_-}^{r_-} \left| \frac{dH}{d\phi} \right|^{-1} (z, \delta) + C_-$$

where r_{\pm} denotes the limits where the hyperbolic expansion is valid and C_{\pm} are small and approximately constant for δ small. Defining a as:

$$\begin{aligned} a_+ &= 2(E-1) \\ a_- &= \frac{2(1-E)}{\Lambda-1}, \end{aligned} \quad (\text{S8})$$

these integrals can be expressed as:

$$\frac{1}{\sqrt{a(\Lambda-1)}} \int_{-r}^r \frac{1}{\sqrt{1-a^{-1}x^2}} dx = \frac{1}{\sqrt{(\Lambda-1)}} \left[\sinh^{-1} \left(\frac{r}{\sqrt{a}} \right) \right] \quad (\text{S9})$$

and for $E \approx 1$, this approximates to as:

$$\begin{aligned} \omega(1+|\delta|)^{-1} &= -\frac{\text{Ln}(|\delta|)}{2\sqrt{(\Lambda-1)}} \\ \omega(1-|\delta|)^{-1} &= -\frac{\text{Ln}(|\delta|)}{\sqrt{(\Lambda-1)}} \end{aligned} \quad (\text{S10})$$

IV) Eigenstate Overlaps and Saddle Point Approximation

To approximate the eigenstate overlap for initial states on the separatrix but away from the fixed points, we expand the energy to linear order in z and ϕ :

$$H = \kappa_1 \phi + \gamma_1 z + E_0 \quad (\text{S11})$$

We first write the coherent state with initial imbalance z' and phase ϕ' as:

$$\rho(N, z', \phi', z, \phi) = \frac{\alpha_z(N, z') \alpha_\phi(N, z')}{\pi} \text{Exp} \left[-\alpha_z(N, z')(z - z')^2 - \alpha_\phi(N, z')(\phi - \phi')^2 \right] \quad (\text{S12})$$

where the inverse variances are:

$$\begin{aligned} \alpha_\phi(J, z') &= \frac{1}{2} J (1 - z'^2) \\ \alpha_z(J, z') &= \frac{2J}{1 - z'^2} \end{aligned} \quad (\text{S13})$$

The eigenstate overlap is then given as:

$$\rho_{diag}(z', \phi', E, s) = \frac{\omega(E)}{\gamma_1} \int d\phi \rho \left(N, z', \phi', \frac{\delta_0 - \kappa_1 \phi}{\gamma}, \phi \right), \quad (\text{S14})$$

where $\delta_0 = E - E_0$. This integrates by parts as:

$$\frac{\omega(E)}{\gamma_1} \frac{\sqrt{\alpha_z(N, z') \alpha_\phi(N, z')}}{\sqrt{\pi} \sqrt{\alpha_\phi + \frac{\kappa_1^2 \alpha_z}{\gamma_1^2}}} \exp \left(-\frac{\delta_0^2 \alpha_\phi \alpha_z}{\gamma_1^2 \alpha_\phi + \kappa_1^2 \alpha_z} \right) \quad (\text{S15})$$

Here we note that the energy uncertainty depends on the coherent state via the uncertainties α_z and α_ϕ . To find long term expectation values, we compute the diagonal ensemble average,

$$O = \int \rho_{diag}(E) O(E), \quad (\text{S16})$$

by performing a saddle point integration in the function ρ_{diag} .

Saddles

Analytic solutions for the saddle point only exist if $E_0 = 1$ so we focus on coherent states on this line. To find the saddle points we rewrite ρ_{diag} as:

$$\rho_{diag}(E = 1 \pm |\delta|) = \frac{K_{\pm}}{(1 - G_{\pm} \text{Ln}[\delta])} \text{Exp}[-2JF\delta^2] \quad (\text{S17})$$

where K_{\pm} and G_{\pm} are constants in δ , depend on C_{\pm} , and with \pm depending on the sign of δ . This function has a saddle at:

$$|\delta| = \frac{i}{\sqrt{(2JF)W_{-1}(-\frac{e^{-2/G_{\pm}}}{F2J})}} \quad (\text{S18})$$

Where the product log, $W_{-1}(X)$, is the inverse of $e^x x$: $W_{-1}(e^x x) = x$ and the $_{-1}$ says to take the negative branch. For small x we get:

$$\lim_{x \rightarrow 0^-} \frac{W_{-1}(x)}{\text{Ln}(x)} = 1 \quad (\text{S19})$$

and we know $W_{-1}(x) \approx \text{Ln}(-x) - \text{Ln}(-\text{Ln}(-x)) + \dots$. We can then write this as:

$$|\delta| = \frac{i}{\sqrt{2JF \text{Ln}(\frac{e^{-2/G_{\pm}}}{F2J})}} \quad (\text{S20})$$

Which in the large- J limit goes as:

$$\frac{1}{\sqrt{2JF \text{Ln}(J)}} \quad (\text{S21})$$

and

$$2JF = \frac{\alpha_{\phi} \alpha_z}{\gamma_1^2 \alpha_{\phi} + \kappa_1^2 \alpha_z} \quad (\text{S22})$$

Thus the difference in initial states on the separatrix again shows up in the scaling to the large J limit. Also note G comes from $W(E)$ which depends on which side of the separatrix we are on (sign of δ). In the large- J limit the points become symmetric as indicated by the lack of dependence on G .

Eigenstate observables close to the separatrix

Next we compute the eigenstate observables, $O(E)$, which are given as

$$W(E) \int O(z, \phi) \delta[H(z, \phi) - E]. \quad (\text{S23})$$

J_z for Λ large has a amazingly simple solution. For $E < 1$, $J_z(E) = 0$ for $E > 1$ we integrate:

$$\int dz \delta[H(z, \phi) - E] = \int_{-\pi}^{\pi} d\phi z(\phi) \left| \frac{dH}{dz} \right|^{-1} \quad (\text{S24})$$

and for $\Lambda \gg 1$, $\left| \frac{dH}{dz} \right|^{-1} \approx \Lambda z$, the z 's cancel and we get

$$J_z(E) = \frac{W(E) 2\pi}{\Lambda}. \quad (\text{S25})$$

J_x is more involved. We will take the same approach as the integral for $\omega(E)$. We assume the integral is dominated by the contribution near the unstable fixed point. Doing so allows us to expand J_x near the unstable fixed point: $J_x \approx -1 + \phi^2/2$. Solving for ϕ , we find that it is written as: $J_x \approx \frac{\Lambda-1}{2} z^2 - E$.

$$\begin{aligned}
J_x(1 + |\delta|)^{-1} &= \omega(E)(\Lambda - 1) \int_{-r_+}^{r_+} \left(-\frac{E}{\Lambda - 1} + z^2/2 \right) \left| \frac{dH}{dz} \right|^{-1} (\phi, \delta) + K_+ \\
J_x(1 - |\delta|)^{-1} &= \omega(E) \int_{-r_-}^{r_-} (-1 + \phi^2/2) \left| \frac{dH}{d\phi} \right|^{-1} (z, \delta) + K_-
\end{aligned} \tag{S26}$$

Similar to the integral for $\omega(E)$, these can be computed and in the limit of small δ we get:

$$\begin{aligned}
J_x(1 + |\delta|)^{-1} &= -1 + \omega(|\delta|) \left(K_+ - \frac{|\delta| \text{Ln}(|\delta|)}{(\Lambda - 1)^{3/2}} \right) \\
J_x(1 - |\delta|)^{-1} &= -1 + \omega(|\delta|) \left(K_- - \frac{|\delta| \text{Ln}(|\delta|)}{\sqrt{\Lambda - 1}} \right)
\end{aligned} \tag{S27}$$

$\omega(|\delta|)$ goes to 0 faster than $\omega(|\delta|) |\delta| \text{Ln}(|\delta|)$ and we get:

$$\begin{aligned}
J_x(1 + |\delta|)^{-1} &= -1 - \omega(|\delta|) \frac{|\delta| \text{Ln}(|\delta|)}{(\Lambda - 1)^{3/2}} \\
J_x(1 - |\delta|)^{-1} &= -1 - \omega(|\delta|) \frac{|\delta| \text{Ln}(|\delta|)}{\sqrt{\Lambda - 1}}
\end{aligned} \tag{S28}$$

Substituting ω :

$$\begin{aligned}
J_x(1 + |\delta|)^{-1} &= -1 + \frac{2|\delta|}{\Lambda - 1} \\
J_x(1 - |\delta|)^{-1} &= -1 + |\delta| \\
J_z(1 + |\delta|) &= \frac{4\pi\sqrt{(\Lambda - 1)}}{\Lambda \text{Ln}(|\delta|)} \\
J_z(1 - |\delta|) &= 0
\end{aligned} \tag{S29}$$

V) Semi-Classical Equilibrium Observables

Using the saddle point values to evaluate the diagonal ensemble observables we get:

$$O_{diag}(z', \phi') = \int \rho_{diag}(E, z', \phi') O(E) = \frac{1}{3} [2O(1 + |\delta|) + O(1 - |\delta|)] \tag{S30}$$

There is a factor of 2 for $+|\delta|$ because $\rho_{diag}(E, z', \phi')$ in the small $|\delta|$ limit is twice as large on the self trapping side (The integral in $\omega(E)$ only integrates over one of the hyperbole on one side of the fixed point while it integrates both sides in the free oscillating limit). This gives the diagonal ensemble observables as:

$$\begin{aligned}
J_z(z', \phi') &= -\frac{8\pi\sqrt{(\Lambda - 1)}}{3\Lambda \text{Ln}(|\delta|(z', \phi'))} \\
J_x(z', \phi') &= -1 + |\delta| \frac{3 + \Lambda}{3(\Lambda - 1)}.
\end{aligned} \tag{S31}$$

By substituting the saddle point location, we get the expressions given in the main text:

$$\begin{aligned}
J_z(z', \phi') &= \frac{4\pi\sqrt{(\Lambda - 1)}}{3\Lambda \text{Ln}[F(z_0, \phi_0)J \text{Ln}[J]]} \\
J_x(z', \phi') &= -1 + \frac{1}{\sqrt{F(z_0, \phi_0)J \text{Ln}[J]}} \frac{3 + \Lambda}{3(\Lambda - 1)}.
\end{aligned} \tag{S32}$$